BIOCHEMISTRY
including biophysical chemistry & molecular biology

Article

pubs.acs.org/biochemistry

Mechanistic Implications of Persulfenate and Persulfide Binding in the Active Site of Cysteine Dioxygenase

Richard J. Souness,[†] Torsten Kleffmann,[‡] Egor P. Tchesnokov,[†] Sigurd M. Wilbanks,[‡] Geoffrey B. Jameson,[§] and Guy N. L. Jameson*[,†]

[†]Department of Chemistry and MacDiarmid Institute for Advanced Materials and Nanotechnology and [‡]Department of Biochemistry, University of Otago, P.O. Box 56, Dunedin 9054, New Zealand

[§]Institute of Fundamental Sciences and MacDiarmid Institute for Advanced Materials and Nanotechnology, Massey University, Private Bag 11 222, Palmerston North 4442, New Zealand

Supporting Information

ABSTRACT: Describing the organization of substrates and substrate analogues in the active site of cysteine dioxygenase identifies potential intermediates in this critical yet poorly understood reaction, the oxidation of cysteine to cysteine sulfinic acid. The fortuitous formation of persulfides under crystallization conditions has allowed their binding in the active site of cysteine dioxygenase to be studied. The crystal structures of cysteine persulfide and 3-mercaptopropionic acid persulfide bound to iron(II) in the active site show that binding of the persulfide occurs via the distal sulfide and, in the case of the cysteine persulfide, the amine also binds. Persulfide was detected by mass spectrometry in both the crystal and the drop, suggesting its origin is chemical rather than enzymatic. A mechanism involving the formation of the relevant disulfide from sulfide produced by hydrolysis of dithionite is proposed. In comparison, persulfenate {observed bound to cysteine dioxygenase [Simmons, C. R., et al. (2008) *Biochemistry 47*, 11390]} is shown through mass spectrometry to occur only in the crystal and not in the surrounding drop, suggesting that in the crystalline state the persulfenate does not lie on the reaction pathway. Stabilization of both the persulfenate and the persulfides does, however, suggest the position in which dioxygen binds during catalysis.

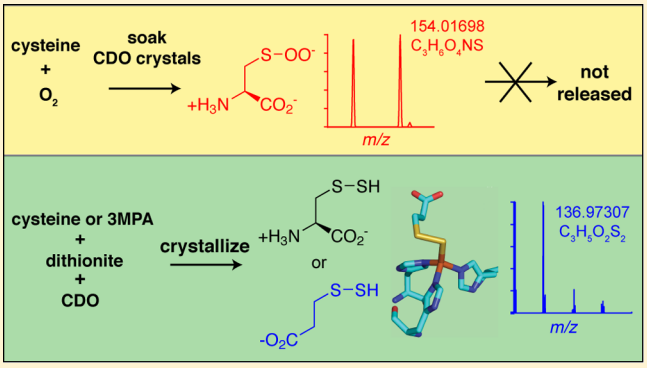

Cysteine dioxygenase (CDO, EC 1.13.11.20) is a non-heme mono-iron enzyme that catalyzes the oxidation of cysteine to cysteine sulfinic acid (CSA) by the addition of the two oxygen atoms from dioxygen to the thiol of cysteine. This enzyme is present in organisms ranging from bacteria to mammals,[1] in which it catalyzes the first step of the removal of sulfur from cysteine to yield taurine or pyruvate. As free cysteine can be cytotoxic[2] and sulfate and taurine are both important for cellular homeostasis, CDO deficiency has been implicated in many disease states, including Parkinson's and Alzheimer's disease.[1,3−5]

CDO differs from other non-heme mono-iron enzymes, limiting the usefulness of comparison to better characterized family members in the mechanistic analysis of CDO. The resting-state iron environment of CDO contains an iron(II) bound to three histidine residues. This complement of ligands differs from the two-histidine, one-carboxylate facial triad that is seen in many of the better studied non-heme mono-iron enzymes.[1,6,7] This unusual neutral suite of ligands for iron(II) is predicted to change the reactivity of cysteine when it is bound to CDO through a change in the overall charge, which influences the Fe−S bond strength.[8] In addition, mammalian CDO contains two post-translational modifications. The first is a cross-link between the thiol of Cys93 and a carbon in the *ortho* position of the phenol of Tyr157.[9−11] The second is a disulfide formed between exogenous cysteine and Cys164.[12] While both modifications have been linked to activity,[9] their mechanistic roles are currently unknown and the second may not be physiological.[12]

Previous investigations have attempted to unravel how these differences affect the structure, kinetic parameters, and catalytic mechanism of CDO. Currently, there are four published crystal structures of mammalian CDO, and two of these structures are of CDO nominally in the resting state.[11,13] The crystal structure of CDO from *Mus musculus* (PDB entry 2atf) contained a catalytically inactive nickel(II) coordinated to the three histidine residues,[13] whereas the crystal structure of CDO from *Rattus norvegicus* (PDB entry 2b5h) contained the catalytically relevant iron(II) (the amino acid sequences of these two structures are identical).[11] In the crystal structure of *R. norvegicus* CDO, Simmons et al. reported that the active site iron has a four-coordinate pseudotetrahedral geometry with a

Received: May 28, 2013
Revised: September 28, 2013
Published: October 1, 2013

very well ordered water molecule taking the fourth coordination site of the iron.[11] This was in contrast with the MCD (*M. musculus*),[14] Mössbauer,[15] and XAS results (*R. norvegicus*),[16] all of which suggested that the iron(II) was in a six-coordinate pseudo-octahedral geometry. However, inspection of electron density maps, using deposited structure factors and coodinates (PDB entry 2bh5), indicates significant residual and unmodeled density in the active site.

The two remaining crystal structures of CDO contain ligands bound to the iron in the active site. Human CDO (sequence 91% identical to that of *R. norvegicus* CDO; PDB entry 2ic1) contained cysteine bound to the iron in a bidentate fashion (via sulfur and nitrogen atoms).[10] This bidentate binding was consistent with results obtained from MCD, resonance Raman,[14] and Mössbauer studies[15] but was inconsistent with XAS data, which suggested no sulfur was bound to the iron.[16] A second *R. norvegicus* crystal structure contained a cysteine persulfenate bound to the iron (PDB entry 3eln). The cysteine-derived portion of the persulfenate bound to the iron in a bidentate fashion, while the dioxygen-derived portion of the persulfenate bound to the iron via only one oxygen atom, in an end-on fashion.[17] The catalytic relevance of the persulfenate is currently unknown. Density functional theory, quantum mechanical/molecular modeling calculations suggested that it is not an energetically favored intermediate in the CDO mechanism. These calculations favored an iron(IV)−oxo intermediate.[18,19]

In addition to the crystal structure of the persulfenate-bound form of CDO, the mode of binding of dioxygen to the active site of CDO has been studied via EPR using the surrogate NO. This study concluded that the dioxygen bound only after the binding of cysteine.[20] Dioxygen binding was also inferred from the ability of superoxide to rescue the catalytically inactive iron(III) substrate-bound form of CDO. While superoxide restored the ability of the enzyme to form CSA, initial turnover was at a much reduced rate compared to that of the steady state of iron(II) CDO with dioxygen.[14] Other non-heme mono-iron enzymes have been shown to undergo a decrease in coordination number upon the binding of substrate, opening a site for binding of dioxygen to the iron and consequent initiation of the catalytic reaction.[21−30] As yet, no studies have convincingly shown the position of binding of dioxygen to the iron of catalytically relevant CDO.

In this work, we investigated further the formation of the persulfenate species reported previously,[17] with the aim of determining whether it lies on the reaction pathway. This we achieved by using mass spectrometry to investigate turnover in the crystalline state. To complement this, we also investigated thiol binding in the absence of dioxygen. The preparation of crystals of *R. norvegicus* CDO in the resting state and in the presence of various sulfur-containing ligands using cocrystallization conditions not previously used fortuitously yielded persulfides of the sulfur-containing ligands (Chart 1). Comparison of these structures with the persulfenate-bound CDO structure allowed us to propose how the active site may stabilize a dioxygen-containing intermediate.

EXPERIMENTAL PROCEDURES

Protein Expression and Purification. The *R. norvegicus* cysteine dioxygenase coding sequence containing a thioredoxin His_6 tag was kindly provided by M. H. Stipanuk (Cornell University, Ithaca, NY). The purification method used here was modified from that reported previously.[9,12,31] Pooled fractions of purified CDO were dialyzed into 50 mM NaCl and 20 mM TRIS (pH 8.0). CDO was enriched with Fe(II) using the same method that was previously reported for Mössbuaer spectroscopy to give a final Fe(II):CDO ratio of 0.91.[15] The concentration was determined from the absorption at 280 nm and the extinction coefficient of 28300 M^{-1} cm^{-1}.[9] Fractions were stored at −80 °C. The full purification protocol and a summary gel of the product resulting from this purification scheme (Figure S1) can be found in the Supporting Information.

Chart 1. Structures of the Molecules Studied

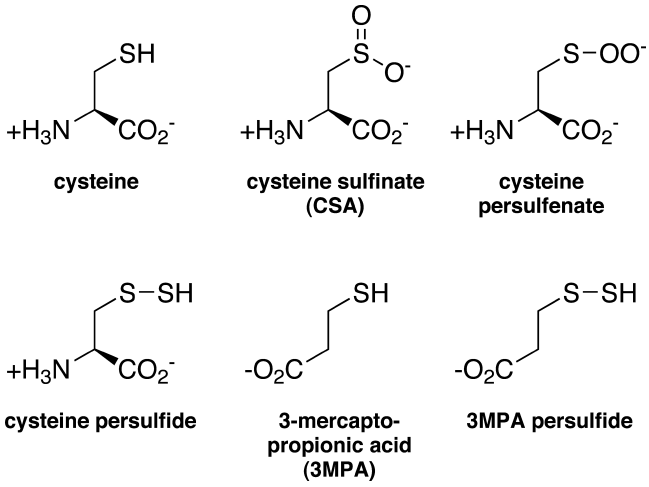

Crystallization and Structure Determination. Crystals were grown aerobically by the hanging-drop vapor-diffusion method in a modification of the procedure of Simmons et al.[11,17,32] Hanging drops (1.5 μL) of approximately 8 mg/mL CDO in the dialysis buffer described above and 1.5 μL of reservoir buffer were allowed to equilibrate above the reservoir buffer [24−34% (w/v) polyethylene glycol 4000, 100−250 mM ammonium acetate, 100 mM sodium citrate (pH 5.6), 0−4 mM dithionite, and 40 mM ligand, as appropriate]. The final pH was 6.1−6.2 (Table S3 of the Supporting Information). The ligands proffered to CDO were cysteine and 3-mercaptopropionic acid (3MPA). Crystals grew as needles or starbursts of approximately 0.1 mm in length at 24 °C in one week. The crystals were analyzed by sodium dodecyl sulfate−polyacrylamide gel electrophoresis (SDS−PAGE) to determine that they contained CDO (Figure S2 of the Supporting Information). To reproduce the persulfenate crystal structure, CDO crystals grown in the absence of ligands were treated as reported by Simmons et al.[17] They were then soaked in 15 μL of an artificial reservoir solution [24% (w/v) polyethylene glycol 4000, 100−250 mM ammonium acetate, and 100 mM sodium citrate (pH 5.6)] with a final cysteine concentration of 100 mM. The final pH was 6.1. Crystals were separated from the rest of the drop and mounted on either a fiber loop or a Mitogen loop and frozen in liquid nitrogen. Diffraction data were collected at the MX1 beamline at the Australian synchrotron via remote operation. MX1 features a silicon double-crystal monochromator and an ADSC Quantum 210R detector. In all cases, 360° of data in 1.0° oscillations were collected with exposure times of 1−3 s per degree with beam attenuation of 80%. The detector was set 160, 175, or 200 mm from the crystal with $2\theta = 0°$; integration of the diffraction data was achieved with iMosflm. Full crystal growth and collection data can be found in Table S1 of the Supporting Information.

dx.doi.org/10.1021/bi400661a | *Biochemistry* 2013, 52, 7606−7617

Table 1. Data Collection and Reduction Statistics for All Fully Refined Data Sets

	resting state	cysteine persulfide bound	3MPA persulfide bound
resolution range (highest shell) (Å)	33.33−1.75 (1.84−1.75)	33.99−1.95 (2.05−1.95)	30.5−1.63 (1.72−1.63)
no. of observed reflections	232683 (44289)	256094 (38076)	143794 (28693)
no. of unique reflections	21688 (3087)	15914 (2257)	26441 (3769)
completeness (%)	100.0 (100.0)	99.9 (99.8)	100.0 (100.0)
redundancy	10.7 (14.3)	16.1 (16.9)	5.4 (7.6)
$I/\sigma(I)$	111.9 (19.7)	67.5 (17.5)	296.1 (27.2)
R_{merge} [a]	0.031 (0.390)	0.042 (0.213)	0.025 (0.362)
Wilson's B factor (Å^2)	18.7	19.2	18.9

[a] $R_{merge} = \sum_h \sum_j |I_{hj}(obs) - \langle I_h \rangle| / \sum_h \sum_j \langle I_h \rangle$.

Table 2. Refinement Data for the Three Fully Refined Crystal Structures

	resting state	cysteine persulfide bound	3MPA persulfide bound
resolution range (highest shell) (Å)	52.12−1.75 (1.79−1.75)	52.25−1.95 (1.99−1.95)	52.06−1.63 (1.67−1.63)
no. of reflections used	20518 (1307)	15053 (948)	24606 (1550)
R_{cryst} [a]	0.20 (0.27)	0.19 (0.21)	0.21 (0.33)
R_{free} [b]	0.22 (0.33)	0.22 (0.24)	0.24 (0.37)
no. of protein, iron, and ligand atoms in model	1557	1578	1571
no. of water molecules in model	160	178	179
rmsd from ideal bond lengths (Å)	0.009	0.010	0.008
rmsd from ideal bond angles (deg)	1.31	1.40	1.26
average B value (Å^2)	19.7	21.5	21.3
average protein B value (Å^2)	18.8	20.6	20.3
average water B value (Å^2)	27.8	29.5	30.1
average ligand B factor (Å^2)	–	26.1	22.0
PDB entry	4kwj	4kwk	4kwl

[a] $R_{cryst} = \sum||F_{obs}| - |F_{calc}|| / \sum|F_{obs}|$ computed over a working set composed of 95% of the data. [b] $R_{free} = \sum||F_{obs}| - |F_{calc}|| / \sum|F_{obs}|$ computed over a test set composed of 5% of the data where the R_{free} set for the 3MPA persulfide derivative contains all those in the R_{free} set for the resting state, which in turn contains all those in the R_{free} set for the cysteine persulfide derivative.

Programs of the CCP4 suite were used for data reduction and analysis.[33] All crystals were indexed in space group $P4_32_12$, with the following unit cell dimensions: $a = b \approx 58$ Å and $c \approx 122$ Å. Unit cell parameters for each set of crystal data are summarized in Table S2 of the Supporting Information. Data collected at the synchrotron were integrated using iMosflm[34] and scaled using Scala.[35] Because the data were very highly redundant, they were ultimately processed with a stringent cutoff for rejection of reflections with outlier intensities. In all cases, the redundancy remained better than 5.4 and the R_{merge} improved considerably. Final data collection and processing statistics are summarized in Table 1.

A set of 5% of reflections was reserved for the calculation of the R_{free} statistics; these reflections were the same as those set aside in the isomorphous structure of PDB entry 3eln.[17] An initial model was obtained by molecular replacement using PDB entry 3eln,[17] stripped of water and persulfenate, as the search model in Phaser.[36] One monomer was placed in the asymmetric unit, and automated model refinement was performed in Refmac 5.6.[37] Models were inspected in COOT,[38] and manual adjustment was performed to match chemical expectations and electron density maps. A final round of refinement in Refmac 5.6 with a weighting on the X-ray term of 0.20 was then performed using no prior phase information. Final refinement details and statistics are summarized in Table 2.

Sample Preparation for Mass Spectrometry. For the mass spectrometry of the cysteine persulfide and 3MPA persulfide-bound crystals, CDO crystals grown in the presence of ligands were placed in 15 μL of 0.4% formic acid and then left to dissolve for 10 min. For parallel analysis of the drop from which crystals had been harvested, after we had checked that no crystals were visible in the drop, 20 μL of 0.4% formic acid was added and the resulting solution was analyzed by mass spectrometry. For the mass spectrometry on the persulfenate-bound crystals, CDO crystals grown in the absence of ligands were soaked in 15 μL of an artificial reservoir solution [24% (w/v) polyethylene glycol 4000, 100−250 mM ammonium acetate, and 100 mM sodium citrate (pH 5.6)] with a final cysteine concentration of 100 mM and no dithionite for 3 h.[17] The crystals were removed from the solution, placed in 15 μL of 0.4% (v/v) formic acid, and then left to dissolve for 10 min. After the crystals were removed from the artificial reservoir solution, 3 μL of the reservoir solution was withdrawn, checked to ensure no crystal fragments were visible, and mixed with 20 μL of 0.4% formic acid to perform mass spectrometry on the solution. All samples were centrifuged at 20000g for 20 min before analysis.

Mass Spectrometry. Liquid chromatography-coupled high-resolution mass spectrometry was performed on a Nanoflow 3000 Ultimate UHPLC system (Dionex, Thermo Scientific, San Diego, CA) inline-coupled to a nanospray ionization source of an LTQ Orbitrap XL mass spectrometer (Thermo Scientific). Samples were diluted 1:2 in water (for negative ion mode) or 0.4% formic acid in water (for positive ion mode) and loaded via a 1 μL loop onto an in-house-packed nanospray emitter-tip column (75 μm inside diameter fused silica tubing with an uncoated tip packed with C_{18} material on a length of 8−9 cm) at a flow rate of 1.5 μL of solvent A (1% acetontrile and 0.2% formic acid in water) per minute. The

dx.doi.org/10.1021/bi400661a | Biochemistry 2013, 52, 7606−7617

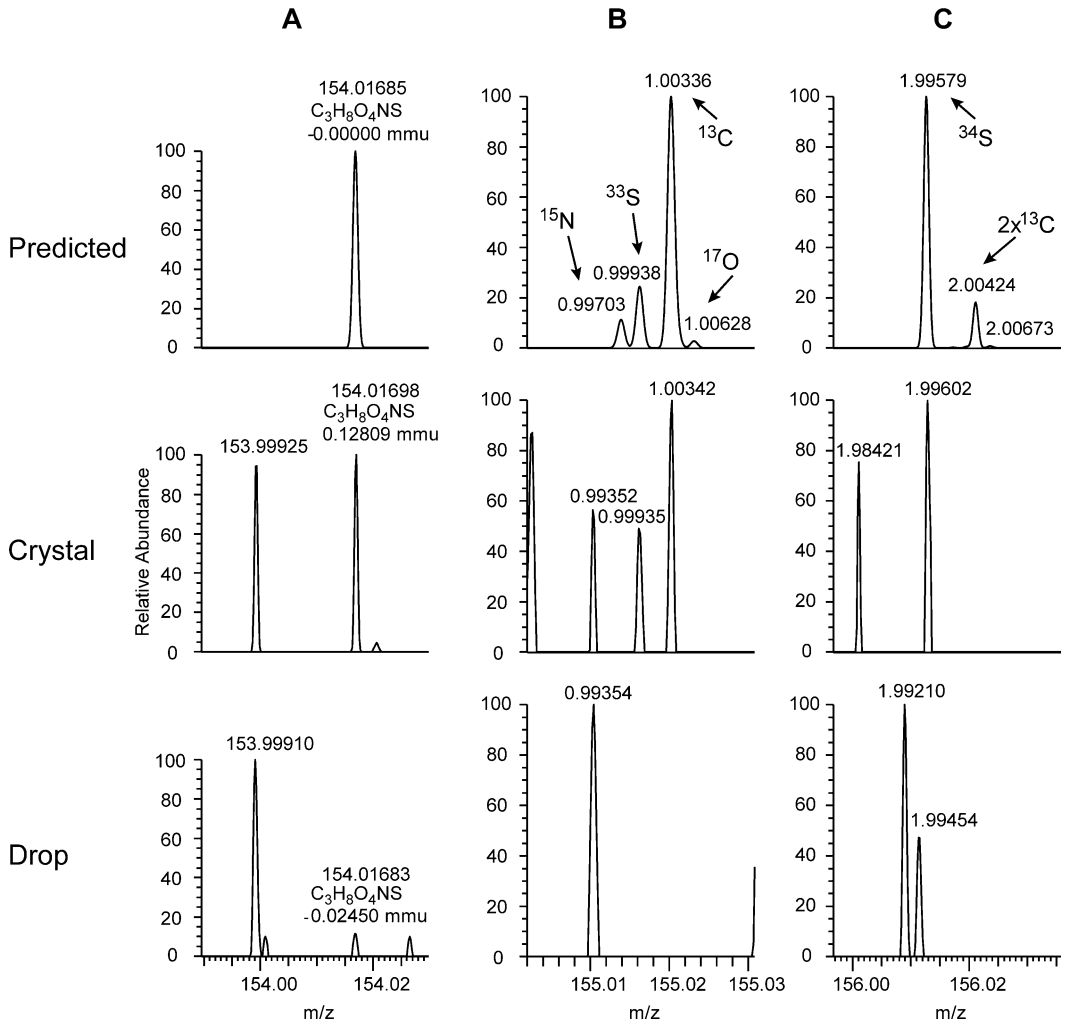

Figure 1. High-resolution mass spectrometry of cysteine persulfenate/cysteine sulfinate. Column A shows a detail of the predicted spectrum for cysteine persulfenate or cysteine sulfinate (predicted) and the spectra measured in the sample extracted from the crystal (crystal) and the drop sample (drop). The monoisotopic peaks are labeled with the predicted or measured mass, the deduced elemental composition, and the mass error in milli-mass units (mmu). Columns B and C show details of the second and third isotope clusters, respectively. The peak labels indicate the mass increments relative to the monoisotopic peak.

hydrophilic compounds were eluted isocratically at the end of the loading phase. The column was then washed with a gradient of 0% solvent B (0.2% formic acid in acetonitrile) to 99% solvent B in solvent A over 7 min and re-equilibrated to 100% solvent A over 3 min. The Orbitrap mass analyzer was operated in either negative (3-MPA derivatives) or positive (cysteine derivatives) ion mode at a resolution of 100000 at m/z 400 for full MS using a narrow mass range of m/z 5 around the precursor masses of interest. Injection waveform was enabled for both the LTQ and Orbitrap mass analyzers. Automated gain control was enabled with targets of 2×10^5 and 2×10^6 for LTQ and Orbitrap MS full scans, respectively. For positive ion mode measurements, the lock mass option was enabled using m/z 445.120025 $\{[Si(CH_3)_2O]_6\}$ as an internal calibrant. For negative ion mode measurements, the default calibration was used. To minimize gas phase oxidation artifacts in the nanospray ion source, ion source settings, such as flow rate, the position of the uncoated emitter tip, and the capillary voltage, were tuned in positive ion mode with a solution of 25 pmol of cysteine/μL of solvent A using the same LC method described above for sample analysis. The capillary voltage was applied to the liquid phase upstream of the emitter tip column. In-source oxidation of cysteine was eliminated almost completely upon application of a capillary voltage of <2 kV at a flow rate of 1.5 μL/min and an emitter tip position directly in front (0−0.5 mm) of the orifice of the ion transfer capillary, which was heated to 180 °C. The optimized ion source settings were used for all sample analyses. All spectra were interpreted manually using Xcalibur (Thermo Scientific, San Jose, CA).

RESULTS

Persulfenate Is Not Released from CDO Crystals. The observation of a stable CDO−cysteine persulfenate complex in crystals suggested only slow, if any, turnover of the enzyme.[17] To assess whether that crystallized complex is catalytically competent, we introduced cysteine into crystals of CDO previously prepared under aerobic conditions, according to the method of Simmons et al.;[17] X-ray diffraction data from these crystals confirmed the published observation of a bound persulfenate (Figure S3 of the Supporting Information).[17] We employed mass spectrometry to confirm the presence of persulfenate in the crystals and assess its presence in the surrounding drop of mother liquor. To avoid misinterpretation of oxidation states due to artificial gas phase oxidation in the

dx.doi.org/10.1021/bi400661a | Biochemistry 2013, 52, 7606−7617

nanospray ion source of the mass spectrometer, we carefully optimized the ion source settings (see Experimental Procedures). Especially high capillary voltages and a position of the uncoated emitter tip more than 0.5 mm from the orifice of the ion transfer capillary caused a significant increase in the level of gas phase oxidation of cysteine to cysteine sulfinate and cysteine sulfonate. Via application of the optimized settings (emitter tip position between 0 and 0.5 mm from the orifice of the ion transfer capillary and a capillary voltage of <2 kV at a flow rate of 1.5 μL/min), no significant in-source oxidation of cysteine was detected (Figure S4 of the Supporting Information). Thus, all oxidation states observed in our sample analyses were generated in solution under the experimental conditions herein described.

In samples of crystals showing persulfenate binding, a clear signal at m/z 154.0167 matching the predicted mass of positively charged cysteine persulfenate or cysteine sulfinate was detectable with an accuracy of ~0.6 ppm after lock mass calibration. Note that the structures of cysteine persulfenate and cysteine sulfinate cannot be distinguished by mass spectrometry alone. The ratios of the isotope peaks containing either ^{15}N, ^{33}S, ^{13}C, ^{34}S, or 2 × ^{13}C are consistent with the most likely elemental composition of $[C_3H_8O_4NS]^+$ (Figure 1). In contrast, no evidence of the persulfenate was found in the drop over the range of the chromatogram (Figure S5 of the Supporting Information), leading us to conclude that under the conditions of its formation, the CDO−persulfenate complex does not turn over. These conditions include the presence of molecular oxygen before and during the diffusion of cysteine into the active site. Furthermore, under these conditions, the enzyme is indeed active, albeit weakly (Table S3 of the Supporting Information).

X-ray Crystal Structure of the Resting State. In view of the discrepancy between the X-ray structure of CDO reported by Simmons et al.[11] and spectroscopic data, the structure of CDO with no sulfur ligand in the reservoir solution was determined to provide a comparison to our persulfide-bound structures (presented below) and to re-evaluate the coordination geometry of the catalytic iron. Although spectroscopic data indicate that iron has an octahedral coordination geometry in the resting state, Simmons et al.[11] reported that the structure contained a tetrahedral iron in the center of the active site bound to three histidine residues and a single well-ordered water molecule. The model obtained from the data collected here (see Tables 1 and 2 for details) is very similar to that reported by Simmons et al.,[11] except for one significant difference. The model presented here (Figure S6 of the Supporting Information) contains a five-coordinate iron in the center of the active site bound to the same three histidine residues, one well-ordered water molecule (B = 13 Å^2), and an additional, less well ordered water molecule (B = 31 Å^2, slightly greater than the average for other water molecules in the structure, B = 27.8 Å^2). Indeed, the electron density maps calculated for our structure and that of Simmons et al.[11] from deposited structure factors (PDB entry 2b5h) are very similar. Omission of this water molecule from the refinement left considerable positive electron density in that position. The difference in B values of the two bound water molecules suggests that the resting state of CDO contains iron(II) in a fluxional coordination environment, consistent with other spectroscopic data.[15,16,20] The model presented here also includes two different conformations of Arg60, suggesting flexibility of this residue in the second coordination sphere in the resting state of CDO. The model matched electron density well in the vicinity of the Cys93−Tyr157 linkage, indicating that the crystal chosen was probably >80% in the linked form, and this is confirmed by SDS−PAGE of the crystals (Figure S2 of the Supporting Information). No unmodeled electron density was observed near Cys164, a site of modification, not always reported, in some CDO structures.

Cocrystallization of CDO with L-Cysteine. To observe alternative binding modes of cysteine, crystals of rat CDO were prepared by the method of Simmons et al.,[11,17,32] modified by the addition of cocrystallant L-cysteine as well as by addition of dithionite intended to prevent oxidation of cysteine residues and of the iron(II) center. Data were collected to 1.95 Å resolution and the structures determined. Information pertaining to data collection and processing can be found in Table 1. In the model, 187 of 200 residues of CDO were resolved and all possessed acceptable geometry. Three residues at the N-terminus and 10 residues at the C-terminus of CDO were not included in the model. The Ramachandran plot of the structure placed 184 residues in allowed positions and the remaining three residues in generously allowed regions. Information about structural models and their refinement can be found in Table 2. The R_{cryst} and R_{free} values were 0.19 and 0.22, respectively. The average B factor was 21.6 Å^2, and the deviation from the ideal bond length was 0.010 Å.

The structure of CDO cocrystallized in the presence of 20 mM cysteine in the reservoir solution has been modeled with a cysteine persulfide at 50% occupancy bound to the iron in the active site (Figure 2). Both small-molecule chemistry[39,40] and macromolecular crystallography[41−44] provide evidence of the existence of persulfides in aqueous solution. The omit map using these diffraction data and a model lacking ligands showed a considerable amount of continuous, unaccounted-for electron density in the active site (Figure S7 of the Supporting Information). Cysteine at approximately 50% occupancy accounted for much of this density but did not explain a spherical peak of electron density slightly higher than that surrounding the cysteine sulfur atom. In the final model, this peak is attributed to the distal sulfur of cysteine persulfide. Mass spectrometry was attempted to provide additional proof, but neither cysteine nor its persulfide was detected, likely because of their neutral overall charge. Evidence against alternate explanations of the crystallographic data is presented in the Supporting Information.

The proximal sulfur (i.e., that derived from the cysteine) interacted with the iron (Fe−S distance of 2.64 Å) and was separated from the putative distal sulfur by a distance typical for a sulfur−sulfur bond (S−S distance of 2.01 Å). The distal sulfur was 2.26 Å from the iron. The cysteine interacted electrostatically with Arg60 (3.28 Å from the carboxylate) and Tyr157 (2.52 Å from the amino group), indicating a role for this tyrosine in positioning the amino acid ligand. The carboxylate group of the cysteine also interacts weakly with Tyr58 (3.39 Å). A water molecule at 50% occupancy (B = 32 Å^2) was added to the left side of the cysteine (as depicted in Figure 2) to complete the active site. This interpretation was validated by the structure of CDO cocrystallized in the presence of 3MPA, where a fully occupied 3MPA persulfide moiety was subsequently unambigously identified by high-resolution mass spectrometry (see below).

Cocrystallization with 3-MPA. To complement attempts to visualize a CDO−cysteine complex, we also investigated the structure of CDO from crystals prepared by cocrystallization of

dx.doi.org/10.1021/bi400661a | Biochemistry 2013, 52, 7606−7617

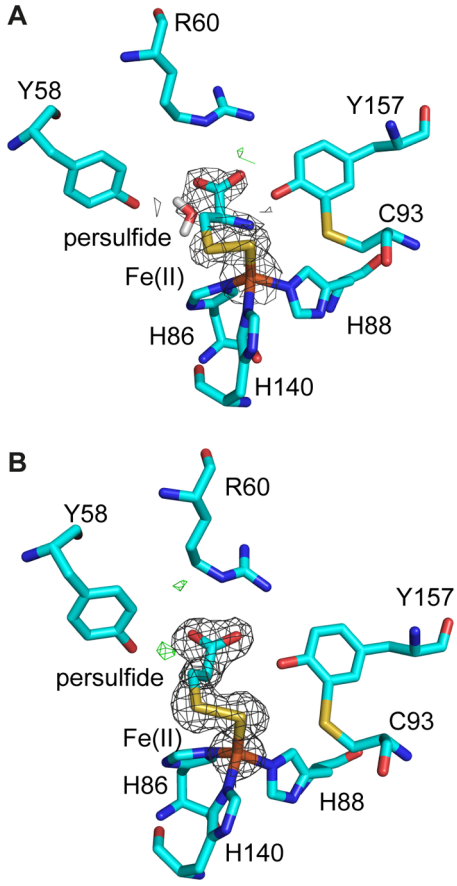

Figure 2. Second coordination sphere of the active sites of the rat CDO crystal structures with persulfide ligands bound to the active site: (A) cysteine persulfide-bound CDO and (B) 3MPA persulfide-bound CDO. In all cases, the $2F_o - F_c$ map (drawn at the 0.8σ contour level for cysteine persulfide and at the 1.0σ contour level for 3MPA persulfide) is the dark gray mesh and the $F_o - F_c$ map (drawn at the $\pm 3.0\sigma$ contour levels) is the green mesh for positive difference electron density and red mesh for negative difference electron density. Atoms are colored as follows: carbon in cyan, nitrogen in blue, oxygen in red, sulfur in yellow, and iron in orange.

CDO in the presence of 3MPA and dithionite. In contrast to the partial occupancy seen in cysteine crystals, full occupancy of the ligand-binding site by a derivative of 3MPA was seen. Initial maps showed two large approximately equal spherical peaks of electron density near the iron(II) center (Figure S8 of the Supporting Information). With coordinated R-S-Cl species excluded (see the rationale in the Supporting Information), there was little choice but to conclude, after sulfenic acid and persulfenate models yielded nonsensical *B* values for sulfenic oxygen atoms, that the species coordinated was the persulfide derivative of 3MPA (Figure 2). This interpretation was validated by subsequent high-resolution mass spectrometry. The proximal sulfur (derived from 3MPA) interacted with the iron (Fe–S distance of 3.24 Å) and was separated from the distal sulfur by a reasonable distance for a sulfur–sulfur bond (S–S distance of 2.08 Å). The distal sulfur was 2.23 Å from the iron, a distance very similar to that seen for the cysteine persulfide derivative. Both sulfur atoms have very similar *B* values of ~17 Å^2, slightly higher than that of the catalytic Fe (12 Å^2). As with the cysteine persulfide, the carboxylate group of 3MPA interacts weakly with Arg60 (3.23 Å), Tyr157 (3.11 Å), and Tyr58 (2.97 Å).

For the pairwise superposition of the three structures, the average rmsd was 0.127 Å. This low value, illustrated in the overlay of the three crystal structures (Figure S9 of the Supporting Information), confirmed that the overall secondary and tertiary structure of CDO was not perturbed by the addition of the various ligands to CDO.

Oxidation State of the Iron. To confirm the oxidation state of the iron, we checked the iron–ligand bond distances (see Table 3). The resting-state CDO is unequivocally Fe(II).

Table 3. Fe–Ligand Bond Distances for Resting-State CDO and Its Cysteine and 3MPA Persulfide Adducts

	Fe–ligand bond distance (Å)		
ligand/species	resting state[a]	3MPA persulfide bound	cysteine persulfide bound
His86	2.01	2.01	2.08
His88	2.07	2.04	2.14
His140	2.07	2.07	2.13
OH_2/S_D[b]	2.12	2.24	2.26
S_G		3.25	2.64
OH_2/NH_2[c]	2.65		2.61

[a]The resting state is unequivocally Fe(II). [b]Water for resting-state CDO; terminal S at this water site for 3MPA persulfide and cysteine persulfide bound to CDO. [c]Water for resting-state CDO; amino group at this water site for cysteine persulfide bound to CDO.

There is no change in Fe–His bonds between resting-state CDO and 3MPA persulfide-bound CDO, but there is a significant lengthening of Fe–His bonds for the cysteine persulfide, consistent with a higher coordination number. Thus, given that resting-state CDO is Fe(II), unambiguously established by Mössbauer spectroscopy, the absence of structural change, especially for the similarly dentated 3MPA persulfide-ligated CDO complex, establishes that the cysteine and 3MPA persulfide species are also Fe(II). The iron site by Fe(II) is clearly fully occupied, because the atomic displacement parameters (*B* values) of the iron and its protein-bound ligands are essentially the same.

Mass Spectrometry Identification of 3-MPA Persulfide. High-resolution mass spectrometry of drop samples and samples extracted from crystals was conducted to independently determine the ligands present in the active site of CDO. Both drop samples and samples of crystals grown in the presence of 3-MPA showed a clear signal at the *m*/*z* value expected for negatively charged 3-MPA persulfide with a mass accuracy of ~3.6 ppm using standard instrument calibration (Figure 3). The isotope peaks of 3-MPA persulfide containing either ^{33}S, ^{13}C, ^{34}S, or 2 × ^{13}C confirmed the presence of two sulfur atoms and the predicted elemental composition of $[C_3H_5O_2S_2]^-$. No accurate mass signal matching for 3-MPA sulfenyl chloride was detectable.

DISCUSSION

Currently, there are three structures with cysteine in the active site,[10,17,45] one of which featuring cysteine persulfenate has been suggested to be an intermediate. We investigated the catalytical relevance of this proposed intermediate during the dioxygenation of cysteine. Unexpectedly, we observed persulfide formation of both cysteine and 3MPA under reducing conditions and stabilization of these molecules in the active site bound to iron. These results provide further insight into the enzyme–substrate interactions of CDO.

dx.doi.org/10.1021/bi400661a | *Biochemistry* 2013, 52, 7606–7617

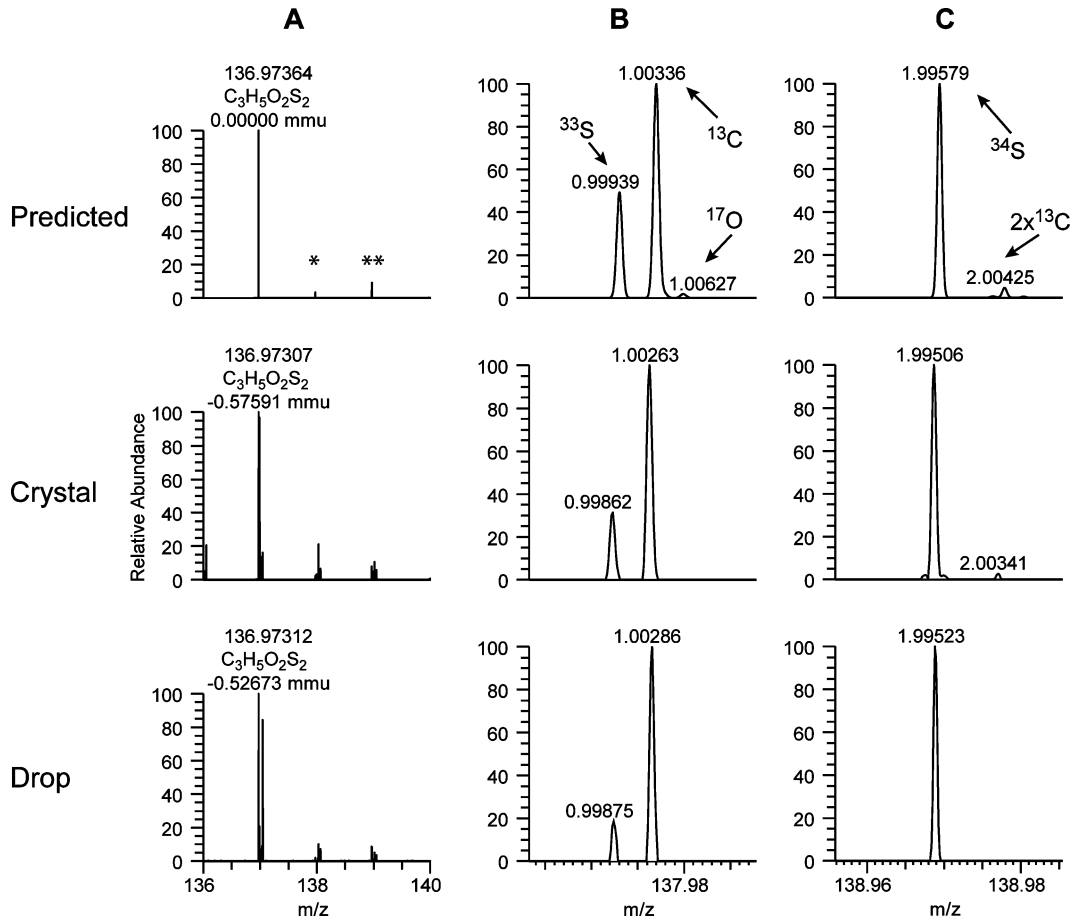

Figure 3. High-resolution mass spectrometry of 3-MPA persulfide. Column A shows the predicted spectrum for 3-MPA persulfide (predicted) and the spectra measured in the sample extracted from the crystal (crystal) and the drop sample (drop). The monoisotopic peaks are labeled with the predicted or measured mass, the deduced elemental composition, and the mass error in milli-mass units (mmu). Columns B and C show enlargements of the second (*) and third (**) isotope clusters, respectively. The peak labels indicate the mass increments relative to the monoisotopic peak.

We reproduced the persulfenate-bound CDO and confirmed the structure by X-ray diffraction. Mass spectrometry was then used to confirm the presence of this species, and the experiments were conducted carefully to ensure that in-source gas phase oxidation of cysteine to its sulfinate[46] was minimized to an insignificant ratio. The mass spectrometry clearly showed the presence of a species with a molecular formula of $C_3H_8O_4NS$ in only the crystals and not in the solution in which the crystals were soaked. This molecular formula is consistent with both the cysteine persulfenate and CSA. The fact that the persulfenate or CSA was identified in only the crystal and not the drop has important implications for the role of the persulfenate in the mechanism of CDO. This result is consistent with two possibilities. The first is that the persulfenate is a stable intermediate of CDO but cannot turn over to yield CSA in the crystalline state. This was suggested by Simmons et al.,[17] but DFT studies of CDO do not agree with this proposal because the reaction pathway with the persulfenate lies significantly higher in energy.[18] Furthermore, protein crystals are known to turn over, albeit slowly,[47] but there is no evidence of any released CSA. The second possibility is that the persulfenate is a side reaction of CDO, which blocks the active site, effectively inhibiting it. The fact that persulfides also bind in the active site could be seen to support this conclusion.

Interestingly, the crystals formed are remarkably stable and could not be redissolved under gentle conditions that would allow the activity to be checked after crystallization. However, the enzyme is active[48] in solution under all the crystallization conditions used, albeit at a significantly lower level (~10%) than at the optimal pH of 8. A very recent publication by Driggers et al.[45] has shown that the persulfenate is produced over a range of pH of 5.5−7.0. At a lower pH (~6), therefore, formation of persulfenate is favored over that of CSA. Moreover, this persulfenate species at a lowered pH does not convert, at least at measurable rates, to the natural product CSA. Rather, cysteine persulfenate remains bound to the enzyme, inhibiting normal CDO activity. It is tempting to suggest a physiological role for this behavior, whereby under conditions of oxidative stress, oxidation of glucose stops at the lactic acid stage, lowering the pH. Formation of a cysteine persulfenate species offers then a quick and metabolically favorable response to decreased oxygen tension, retaining CDO and stopping diversion of dioxygen needed for primary metabolism into the oxidation of cysteine to CSA, until such time as the oxygen tension and pH return to normal.

Previous work investigating the binding of cysteine to CDO using electronic absorption,[20] MCD,[20] and stopped flow[15] has shown that there is a considerable difference between CDO−Fe^{II}−cysteine and CDO−Fe^{III}−cysteine complexes, with the

dx.doi.org/10.1021/bi400661a | *Biochemistry* 2013, 52, 7606−7617

ferrous form known to be the only active form. Single-turnover experiments (data not shown) have shown that CDO is capable of using the low levels of dioxygen in our glovebox (~1 ppm). This high reactivity for dioxygen has precedence and has been observed in the same make of glovebox for another non-heme mono-iron enzyme, HPCD.[47] Dithionite was therefore added to the reservoir solution to ensure the iron site was reduced to Fe(II), to remove dioxygen from the solution, and to prevent the formation of disulfide bonds between ligands, a process that is extremely facile at near-neutral pH. Under these conditions, we hoped to crystallize the cysteine-bound form of rat CDO that has eluded researchers until recently,[45] but instead, persulfides bound to the iron were observed. Cysteine persulfides have previously been observed in macromolecular crystallography in a number of different proteins,[42−44,49] although not coordinated to a non-heme mono-iron enzyme as in this case. Moreover, this is the first time 3MPA persulfide has been reported in the PDB. Interestingly, crystals grown in the absence of dithionite were of low quality compared to those grown in its presence, and crystallographic data were not collected.

Assignment of the iron-coordinating ligand in our CDO crystals was confirmed using mass spectrometry, which detected the presence of the 3MPA persulfide in both the crystals and the drop in which they were grown. Because of the unfortunate neutralization of charge caused by the extra amine that prohibited detection by mass spectrometry, cysteine persulfide was not observed directly. However, the 3MPA data strongly support this assignment. Because the persulfide was found in both the drop and the crystal, it was concluded that the persulfide was formed chemically, rather than enzymatically. This is supported by previous NMR assays of the catalytic turnover of CDO, where no persulfide was observed in the absence of dithionite.[48]

Comparison of crystallization conditions that did produce persulfides with those that did not suggests that the formation of persulfides involves the reaction between thiol and dithionite. Dithionite supports heterolytic cleavage of disulfide bonds at neutral pH[50] and produces sulfides due to alkaline hydrolysis.[51] Recently, it has been shown that hydrogen sulfide can react with disulfides to produce persulfides.[52] The mass spectrometry results presented here suggest that there are large amounts of 3MPA disulfide present (Figure S10 of the Supporting Information), so although crystallization occurred at a pH (6.1−6.3) where the level of sulfide production from hydrolysis of dithionite would be expected to be low, this series of nucleophilic reactions (see Scheme 1) could explain the formation of the persulfide, especially considering the length of time of crystallization (approximately 2 weeks) and the thermodynamic pull of sequestering the persulfide to the iron(II) of CDO. While a radical-based reaction cannot be discounted, the scenario described above has precedent.

Scheme 1. Plausible Reaction Scheme Whereby the Persulfide Is Formed under the Crystallization Conditions of Cysteine Dioxygenase Described in the Text

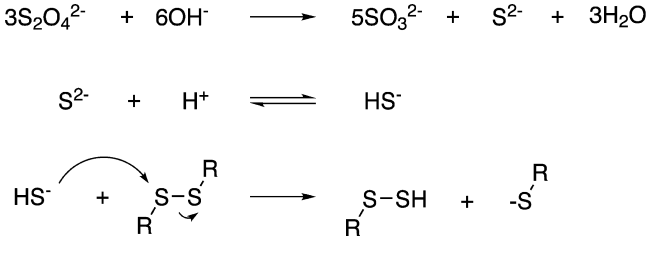

The orientation of the cysteine persulfide bound in CDO was much closer to the orientation of the persulfenate in the crystal structure by Simmons et al. than that of cysteine in the human cysteine-bound crystal structure of Ye et al.[10,17] This was expected as the geometry of the iron in both the persulfenate and persulfide crystal structures is pseudo-octahedral. In contrast, the crystal structure of Ye et al. contained the iron(II) in a pseudotrigonal bipyramidal geometry. The pseudo-octahedral geometry shown by the rat CDO structures presented here and previously provides useful insight into the binding of dioxygen at the active site. The fact that both the persulfide and persulfenate form complexes with CDO suggests that the active site favors this orientation. Cysteine oxidation in small-molecule model systems[53−56] has been shown to require the thiolate and dioxygen to bind *cis* to each other. Removal of the distal sulfur (in the case of the persulfide structure) and the dioxygen (in the case of the persulfenate) allows the iron to more clearly display a spare coordination site for the binding of dioxygen. Therefore, these persulfide and persulfenate crystal structures are probably more indicative of the catalytic orientation of cysteine in the active site of CDO than that reported in the crystal structure by Ye et al. (Figure 4), where the low resolution (2.70 Å) precludes the unequivocal determination of orientation seen for exogenous ligands in our higher-resolution structures. This conclusion was recently drawn independently by Diggers et al.[45]

Both the cysteine persulfide and persulfenate[17] structures showed close interactions between their respective amines and the phenol of Tyr157. The presence of an *ortho* substituent on phenol has been shown to lower the pK_a of the phenol.[57,58] This would give the Cys93−Tyr157 cross-link a role in the mechanism of CDO: to facilitate the deprotonated Tyr157 to operate in a wider variety of environments, allowing it to abstract a proton from the amine (-NH_3^+) of cysteine, aiding substrate binding, and thereby increasing the rate of reaction.[9,59]

The bacterial enzyme 3-mercaptopropionic acid dioxygenase (3MDO)[60] has been shown to be capable of oxidizing 3MPA but not cysteine. The specificity of thiol dioxygenases[61] is indeed remarkable, and CDO itself is inhibited by 3MPA.[16] 3MDO is a homologue of CDO with the same three-histidine iron-binding motif of CDO, but the structurally equivalent position of Arg60 is occupied by a glutamine. This indicates the importance of second-coordination sphere interactions in CDO through Arg60 and Tyr157 with the carboxyl group and amine, respectively, and shows the importance of the amine group in orienting cysteine correctly for reaction. The lack of an amine in 3MPA may strengthen the influence of the electrostatic interactions between Arg60 and the 3MPA carboxylate in CDO and move 3MPA away from the iron. Indeed, the 3MPA persulfide structure presented here suggests that 3MPA may only form a sulfur−iron bond when present as a persulfide; for the cysteine persulfide and 3MPA persulfide structures, the proximal Fe−S separations are 2.6 and 3.2 Å, respectively, while the distal Fe−S separation remains the same at 2.3 Å. This observation is supported by a Mössbauer spectrum of CDO in the presence of 10 mM 3MPA (and in the absence of dithionite). Little change in the Mössbauer spectrum is observed upon addition of 3MPA compared to that of the resting state (Figure S11 of the Supporting Information),

dx.doi.org/10.1021/bi400661a | *Biochemistry* 2013, 52, 7606−7617

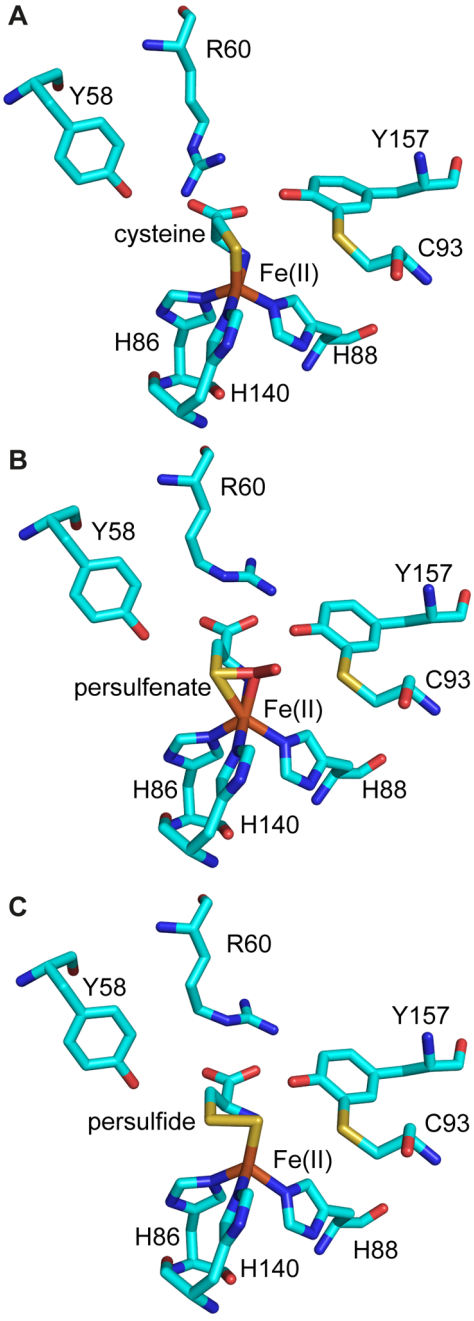

Figure 4. Comparison of the second coordination sphere of the active site of CDO with species bound in the active site: (A) cysteine-bound CDO by Ye et al. (PDB entry 2ic1[10]), (B) cysteine persulfenate-bound CDO (PDB entry 3eln[17]), and (C) L-cysteine persulfide-bound CDO. Atoms are colored as in Figure 2.

indicating that there is little interaction between the Fe(II) of CDO and 3MPA. This is in stark contrast to the substantial changes in spectra caused by the presence of cysteine or homocysteine.[15]

The crystal structures presented also throw light on substrate binding by the non-heme mono-iron enzyme persulfide oxidase (ETHE1), which oxidizes persulfides into sulfite and a thiolate in the mitochondria.[62] This enzyme appears to play an important role in the metabolism of hydrogen sulfide; the importance of this molecule as a cell-signaling agent has recently been recognized.[63,64] The enzyme is a non-heme mono-iron enzyme, and its active site contains an iron(II) coordinated to two histidine residues and a carboxylate residue. ETHE1 has not yet been crystallized, but characterization of a protein from *Arabidopsis thaliana* that has a sequence 54% identical to that of ETHE1 and shares a similar active site has recently been published.[65] Subsequent modeling of ETHE1 has been performed on the basis of this structure, but the ligand is not present in these structures.[62] The structures of persulfide-bound species to CDO presented here can be overlaid (Figure 5) and usefully compared with that of the ETHE1-type protein

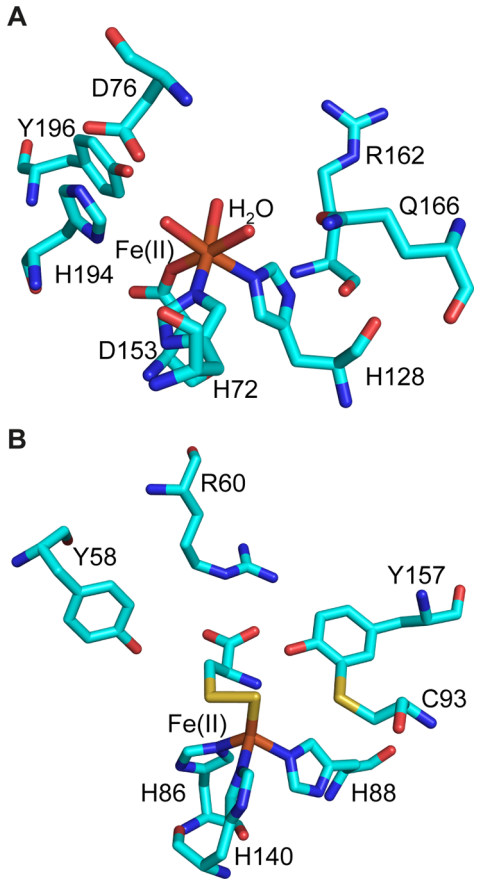

Figure 5. Comparison of the second coordination sphere of the active sites of the ETHE1-like protein from *A. thaliana* and rat CDO. (A) Active sites of the ETHE1-like protein from *A. thaliana*. Note the volume of the larger binding pocket is greatly reduced if Arg162 is projected into the pocket, as might occur upon binding of small anionic subtrates. From PDB entry 2gcu.[65] (B) Cysteine persulfide-bound CDO. Atoms are colored as in Figure 2.

from *A. thaliana*, suggesting a binding mode for the substrates of ETHE1. In both of the CDO structures, the cysteine persulfide or the 3MPA persulfide is bound to the iron via the distal sulfur. The proximal sulfur is close enough to interact with the iron, but not close enough to formally bind. The cysteine persulfide amine loosely binds to the iron to form a chelate. This type of binding supports the mode of binding of persulfides to the iron in ETHE1 proposed by Kabil et al.[62] In the case of mammalian CDO, the facile formation of persulfide species by dithionite indicates that nature carefully controls access of cysteine to sulfide transfer agents, such as H_2S, in the cell.

dx.doi.org/10.1021/bi400661a | *Biochemistry* 2013, 52, 7606−7617

CONCLUSION

The observation of robust active-site binding by persulfides, although most likely chemically formed, adds weight to the idea that the persulfenate structure could be more than just a crystallographic anomaly. The active site is able to stabilize the persulfides in the active site, and the structures are remarkably similar to the persulfenate structure. However, we obtained mass spectrometry data suggesting that the persulfentate complex does not appear to be a significant catalytic intermediate. Although these investigations did not trap a reactive intermediate able to produce CSA, altogether, these data weaken the case for the persulfenate as an on-pathway intermediate but strengthen the case for an intermediate with a single atom of dioxygen bound to an octahedrally coordinated iron.

ASSOCIATED CONTENT

Supporting Information

Full purification protocols, identification of ligands, Mössbauer spectroscopy protocols, SDS−PAGE gel of the purification summary and crystals used, full crystal growth and collection data, cell dimensions, optimized ion source conditions, crystal structures, omit maps, extracted ion chromatograms, Mössbauer spectra, and activity data. This material is available free of charge via the Internet at http://pubs.acs.org.

AUTHOR INFORMATION

Corresponding Author

*Department of Chemistry, University of Otago, P.O. Box 56, Dunedin 9054, New Zealand. Telephone: +64 3 479 8028. E-mail: gjameson@chemistry.otago.ac.nz.

Funding

This work was supported by the Marsden Fund of the Royal Society of New Zealand (G.N.L.J., Principal Investigator; S.M.W., Associate Investigator). R.J.S. was the recipient of a TEC Top Achiever Doctoral Scholarship. E.P.T. was supported by a Canadian Health Research Postdoctoral Fellowship.

Notes

The authors declare no competing financial interest.

ACKNOWLEDGMENTS

We thank Matthias Fellner for collecting the activity data.

ABBREVIATIONS

CDO, cysteine dioxygenase; CSA, cysteinesulfinic acid; PDB, Protein Data Bank; MCD, magnetic circular dichroism; XAS, X-ray absorption spectroscopy; EPR, electron paramagnetic resonance; 3MPA, 3-mercaptopropionic acid; DFT, density functional theory; ETHE1, enzyme persulfide oxidase; rmsd, root-mean-square deviation.

REFERENCES

(1) Joseph, C. A., and Maroney, M. J. (2007) Cysteine dioxygenase: Structure and mechanism. *Chem. Commun.*, 3338−3349.

(2) Dominy, J. E., Hwang, J., and Stipanuk, M. H. (2007) Overexpression of cysteine dioxygenase reduces intracellular cysteine and glutathione pools in HepG2/C3A cells. *Am. J. Physiol. 293*, E62−E69.

(3) Jameson, G. N. L. (2011) Iron, cysteine and Parkinson's disease. *Monatsh. Chem. 142*, 325−329.

(4) Jameson, G. N. L., Zhang, J., Jameson, R. F., and Linert, W. (2004) Kinetic evidence that cysteine reacts with dopaminoquinone via reversible adduct formation to yield 5-cysteinyl-dopamine: An important precursor of neuromelanin. *Org. Biomol. Chem. 2*, 777−782.

(5) Heafield, M. T., Fearn, S., Steventon, G. B., Waring, R. H., Williams, A. C., and Sturman, S. G. (1990) Plasma cysteine and sulphate levels in patients with motor neurone, Parkinson's and Alzheimer's disease. *Neurosci. Lett. 110*, 216−220.

(6) Hegg, E. L., and Que, L., Jr. (1997) The 2-His-1-carboxylate facial triad. *Eur. J. Biochem. 250*, 625−629.

(7) Costas, M., Mehn, M. P., Jensen, M. P., and Que, L. (2004) Dioxygen Activation at Mononuclear Nonheme Iron Active Sites: Enzymes, Models, and Intermediates. *Chem. Rev. 104*, 939−986.

(8) de Visser, S. P., and Straganz, G. D. (2009) Why Do Cysteine Dioxygenase Enzymes Contain a 3-His Ligand Motif Rather than a 2His/1Asp Motif Like Most Nonheme Dioxygenases? *J. Phys. Chem. A 113*, 1835−1846.

(9) Siakkou, E., Rutledge, M. T., Wilbanks, S. M., and Jameson, G. N. L. (2011) Correlating crosslink formation with enzymatic activity in cysteine dioxygenase. *Biochim. Biophys. Acta 1814*, 2003−2009.

(10) Ye, S., Wu, X., Wei, L., Tang, D., Sun, P., Bartlam, M., and Rao, Z. (2007) An Insight into the Mechanism of Human Cysteine Dioxygenase: Key Roles of the Thioether-Bonded Tyrosine-Cysteine Cofactor. *J. Biol. Chem. 282*, 3391−3402.

(11) Simmons, C. R., Liu, Q., Huang, Q. Q., Hao, Q., Begley, T. P., Karplus, P. A., and Stipanuk, M. H. (2006) Crystal structure of mammalian cysteine dioxygenase: A novel mononuclear iron center for cysteine thiol oxidation. *J. Biol. Chem. 281*, 18723−18733.

(12) Kleffmann, T., Jongkees, S. A. K., Fairweather, G., Wilbanks, S. M., and Jameson, G. N. L. (2009) Mass-spectrometric characterization of two posttranslational modifications of cysteine dioxygenase. *JBIC, J. Biol. Inorg. Chem. 14*, 913−321.

(13) McCoy, J. G., Bailey, L. J., Bitto, E., Bingman, C. A., Aceti, D. J., Fox, B. G., and Phillips, G. N. (2006) Structure and mechanism of mouse cysteine dioxygenase. *Proc. Natl. Acad. Sci. U.S.A. 103*, 3084−3089.

(14) Crawford, J. A., Li, W., and Pierce, B. S. (2011) Single Turnover of Substrate-Bound Ferric Cysteine Dioxygenase with Superoxide Anion: Enzymatic Reactivation, Product Formation, and a Transient Intermediate. *Biochemistry 50*, 10241−10253.

(15) Tchesnokov, E. P., Wilbanks, S. M., and Jameson, G. N. L. (2012) A Strongly Bound High-Spin Iron(II) Coordinates Cysteine and Homocysteine in Cysteine Dioxygenase. *Biochemistry 51*, 257−264.

(16) Chai, S. C., Bruyere, J. R., and Maroney, M. J. (2006) Probes of the catalytic site of cysteine dioxygenase. *J. Biol. Chem. 281*, 15774−15779.

(17) Simmons, C. R., Krishnamoorthy, K., Granett, S. L., Schuller, D. J., Dominy, J. E., Begley, T. P., Stipanuk, M. H., and Karplus, P. A. (2008) A Putative Fe^{2+}-Bound Persulfenate Intermediate in Cysteine Dioxygenase. *Biochemistry 47*, 11390−11392.

(18) Kumar, D., Thiel, W., and de Visser, S. P. (2011) Theoretical Study on the Mechanism of the Oxygen Activation Process in Cysteine Dioxygenase Enzymes. *J. Am. Chem. Soc. 133*, 3869−3882.

(19) Aluri, S., and de Visser, S. P. (2007) The Mechanism of Cysteine Oxygenation by Cysteine Dioxygenase Enzymes. *J. Am. Chem. Soc. 129*, 14846−14847.

(20) Gardner, J. D., Pierce, B. S., Fox, B. G., and Brunold, T. C. (2010) Spectroscopic and Computational Characterization of Substrate-Bound Mouse Cysteine Dioxygenase: Nature of the Ferrous and Ferric Cysteine Adducts and Mechanistic Implications. *Biochemistry 49*, 6033−6041.

(21) Davis, M. I., Wasinger, E. C., Decker, A., Pau, M. Y. M., Vaillancourt, F. H., Bolin, J. T., Eltis, L. D., Hedman, B., Hodgson, K. O., and Solomon, E. I. (2003) Spectroscopic and Electronic Structure Studies of 2,3-Dihydroxybiphenyl 1,2-Dioxygenase: O_2 Reactivity of the Non-Heme Ferrous Site in Extradiol Dioxygenases. *J. Am. Chem. Soc. 125*, 11214−11227.

(22) Ohta, T., Chakrabarty, S., Lipscomb, J. D., and Solomon, E. I. (2008) Near-IR MCD of the Nonheme Ferrous Active Site in Naphthalene 1,2-Dioxygenase: Correlation to Crystallography and

Structural Insight into the Mechanism of Rieske Dioxygenases. *J. Am. Chem. Soc. 130*, 1601−1610.
(23) Shu, L., Chiou, Y.-M., Orville, A. M., Miller, M. A., Lipscomb, J. D., and Que, L. (1995) X-ray absorption spectroscopic studies of the Fe(II) active site of catechol 2,3-dioxygenase. Implications for the extradiol cleavage mechanism. *Biochemistry 34*, 6649−6659.
(24) Elkins, J. M., Ryle, M. J., Clifton, I. J., Dunning Hotopp, J. C., Lloyd, J. S., Burzlaff, N. I., Baldwin, J. E., Hausinger, R. P., and Roach, P. L. (2002) X-ray Crystal Structure of *Escherichia coli* Taurine/α-Ketoglutarate Dioxygenase Complexed to Ferrous Iron and Substrates. *Biochemistry 41*, 5185−5192.
(25) Diebold, A. R., Neidig, M. L., Moran, G. R., Straganz, G. D., and Solomon, E. I. (2010) The Three-His Triad in Dke1: Comparisons to the Classical Facial Triad. *Biochemistry 49*, 6945−6952.
(26) Roach, P. L., Clifton, I. J., Fulop, V., Harlos, K., Barton, G. J., Hajdu, J., Andersson, I., Schofield, C. J., and Baldwin, J. E. (1995) Crystal structure of isopenicillin *N* synthase is the first from a new structural family of enzymes. *Nature 375*, 700−704.
(27) Roach, P. L., Clifton, I. J., Hensgens, C. M. H., Shibata, N., Schofield, C. J., Hajdu, J., and Baldwin, J. E. (1997) Structure of isopenicillin N synthase complexed with substrate and the mechanism of penicillin formation. *Nature 387*, 827−830.
(28) Valegard, K., van Scheltinga, A. C. T., Lloyd, M. D., Hara, T., Ramaswamy, S., Perrakis, A., Thompson, A., Lee, H. J., Baldwin, J. E., Schofield, C. J., Hajdu, J., and Andersson, I. (1998) Structure of a cephalosporin synthase. *Nature 394*, 805−809.
(29) Zhou, J., Kelly, W. L., Bachmann, B. O., Gunsior, M., Townsend, C. A., and Solomon, E. I. (2001) Spectroscopic Studies of Substrate Interactions with Clavaminate Synthase 2, a Multifunctional α-KG-Dependent Non-Heme Iron Enzyme: Correlation with Mechanisms and Reactivities. *J. Am. Chem. Soc. 123*, 7388−7398.
(30) Pavel, E. G., Zhou, J., Busby, R. W., Gunsior, M., Townsend, C. A., and Solomon, E. I. (1998) Circular Dichroism and Magnetic Circular Dichroism Spectroscopic Studies of the Non-Heme Ferrous Active Site in Clavaminate Synthase and Its Interaction with α-Ketoglutarate Cosubstrate. *J. Am. Chem. Soc. 120*, 743−753.
(31) Simmons, C. R., Hirschberger, L. L., Machi, M. S., and Stipanuk, M. H. (2006) Expression, purification, and kinetic characterization of recombinant rat cysteine dioxygenase, a non-heme metalloenzyme necessary for regulation of cellular cysteine levels. *Protein Expression Purif. 47*, 74−81.
(32) Simmons, C. R., Hao, Q., and Stipanuk, M. H. (2005) Preparation, crystallization and X-ray diffraction analysis to 1.5 angstrom resolution of rat cysteine dioxygenase, a mononuclear iron enzyme responsible for cysteine thiol oxidation. *Acta Crystallogr. F61*, 1013−1016.
(33) Collaborative Computational Project, number 4 (1994) The CCP4 suite: Programs for protein crystallography. *Acta Crystallogr. D50*, 760−763.
(34) Read, R. J., and Sussman, J. L. (2007) Processing diffraction data with mosflm. In *Evolving Methods for Macromolecular Crystallography* (Read, R. J., and Sussman, J. L., Eds.) pp 41−51, Springer, Dordrecht, The Netherlands.
(35) Evans, P. (2006) Scaling and assessment of data quality. *Acta Crystallogr. D62*, 72−82.
(36) McCoy, A. J., Grosse-Kunstleve, R. W., Adams, P. D., Winn, M. D., Storoni, L. C., and Read, R. J. (2007) Phaser crystallographic software. *J. Appl. Crystallogr. 40*, 658−674.
(37) Murshudov, G. N., Vagin, A. A., and Dodson, E. J. (1997) Refinement of Macromolecular Structures by the Maximum-Likelihood Method. *Acta Crystallogr. D53*, 240−255.
(38) Emsley, P., Lohkamp, B., Scott, W. G., and Cowtan, K. (2010) Features and development of Coot. *Acta Crystallogr. D66*, 486−501.
(39) Silber, P. (1975) Crystal structure of potassium perthiocarbonate monomethanolate. *Rev. Chim. Miner. 12*, 347.
(40) Krautscheid, U. (1993) N-Methylimidazole mediated chemistry of transition metal phenylthiolates. The isolation of the perthiolate salts $[M(N\text{-}MeIm)_6](S_2Ph)_2$. *Z. Naturforsch. B 48*, 653.
(41) Veith, A., Urich, T., Seyfarth, K., Protze, J., Frazão, C., and Kletzin, A. (2011) Substrate pathways and mechanisms of inhibition in the sulfur oxygenase reductase of *Acidianus ambivalens*. *Front. Microbiol. 2*, 1−12.
(42) Bamford, V. A., Bruno, S., Rasmussen, T., Appia-Ayme, C., Cheesman, M. R., Berks, B. C., and Hemmings, A. M. (2002) Structural basis for the oxidation of thiosulfate by a sulfur cycle enzyme. *EMBO J. 21*, 5599−5610.
(43) Lima, C. D. (2002) Analysis of the *E. coli* NifS CsdB protein at 2.0 Å reveals the structural basis for perselenide and persulfide intermediate formation. *J. Mol. Biol. 315*, 1199−1208.
(44) Clausen, T., Kaiser, J. T., Steegborn, C., Huber, R., and Kessler, D. (2000) Crystal structure of the cystine C-S lyase from *Synechocystis*: Stabilization of cysteine persulfide for FeS cluster biosynthesis. *Proc. Natl. Acad. Sci. U.S.A. 97*, 3856−3861.
(45) Driggers, C. M., Cooley, R. B., Sankaran, B., Hirschberger, L. L., Stipanuk, M. H., and Karplus, P. A. (2013) Cysteine Dioxygenase Structures from pH 4 to 9: Consistent Cys-Persulfenate Formation at Intermediate pH and a Cys-Bound Enzyme at Higher pH. *J. Mol. Biol. 425*, 3121−3136.
(46) Boys, B. L., Kuprowski, M. C., NoeÃàl, J. J., and Konermann, L. (2009) Protein Oxidative Modifications During Electrospray Ionization: Solution Phase Electrochemistry or Corona Discharge-Induced Radical Attack? *Anal. Chem. 81*, 4027−4034.
(47) Kovaleva, E. G., and Lipscomb, J. D. (2007) Crystal Structures of Fe^{2+} Dioxygenase Superoxo, Alkylperoxo, and Bound Product Intermediates. *Science 316*, 453−457.
(48) Siakkou, E., Wilbanks, S. M., and Jameson, G. N. L. (2010) Simplified cysteine dioxygenase activity assay allows simultaneous quantitation of both substrate and product. *Anal. Biochem. 405*, 127−131.
(49) Urich, T., Gomes, C. M., Kletzin, A., and Frazão, C. (2006) X-ray Structure of a Self-Compartmentalizing Sulfur Cycle Metalloenzyme. *Science 311*, 996−1000.
(50) Knipp, M., Taing, J. J., and He, C. (2011) Reduction of the lipocalin type heme containing protein nitrophorin: Sensitivity of the fold-stabilizing cysteine disulfides toward routine heme-iron reduction. *J. Inorg. Biochem. 105*, 1405−1412.
(51) Kilroy, W. P. (1980) Anaerobic decomposition of sodium dithionite in alkaline solution. *J. Inorg. Nucl. Chem. 42*, 1071−1073.
(52) Francoleon, N. E., Carrington, S. J., and Fukuto, J. M. (2011) The reaction of H_2S with oxidized thiols: Generation of persulfides and implications to H_2S biology. *Arch. Biochem. Biophys. 516*, 146−153.
(53) Badiei, Y. M., Siegler, M. A., and Goldberg, D. P. (2011) O_2 Activation by Bis(imino)pyridine Iron(II)−Thiolate Complexes. *J. Am. Chem. Soc. 133*, 1274−1277.
(54) Jiang, Y., Widger, L. R., Kasper, G. D., Siegler, M. A., and Goldberg, D. P. (2010) Iron(II)-Thiolate S-Oxygenation by O_2: Synthetic Models of Cysteine Dioxygenase. *J. Am. Chem. Soc. 132*, 12214−12215.
(55) Kumar, D., Sastry, G. N., Goldberg, D. P., and de Visser, S. P. (2012) Mechanism of S-Oxygenation by a Cysteine Dioxygenase Model Complex. *J. Phys. Chem. A 116*, 582−591.
(56) McQuilken, A. C., Jiang, Y., Siegler, M. A., and Goldberg, D. P. (2012) Addition of Dioxygen to an N_4S(thiolate) Iron(II) Cysteine Dioxygenase Model Gives a Structurally Characterized Sulfinato−Iron(II) Complex. *J. Am. Chem. Soc. 134*, 8758−8761.
(57) Himo, F., Noodleman, L., Blomberg, M. R. A., and Siegbahn, P. E. M. (2002) Relative Acidities of Ortho-Substituted Phenols, as Models for Modified Tyrosines in Proteins. *J. Phys. Chem. A 106*, 8757−8761.
(58) Whittaker, M. M., Chuang, Y. Y., and Whittaker, J. W. (1993) Models for the redox active site in galactose oxidase. *J. Am. Chem. Soc. 115*, 10029−10035.
(59) Dominy, J. E., Jr., Hwang, J., Guo, S., Hirschberger, L. L., Zhang, S., and Stipanuk, M. H. (2008) Synthesis of Amino Acid Cofactor in Cysteine Dioxygenase Is Regulated by Substrate and Represents a

Novel Post-translational Regulation of Activity. *J. Biol. Chem. 283*, 12188−12201.
(60) Bruland, N., Wubbeler, J. H., and Steinbuchel, A. (2009) 3-Mercaptopropionate Dioxygenase, a Cysteine Dioxygenase Homologue, Catalyzes the Initial Step of 3-Mercaptopropionate Catabolism in the 3,3-Thiodipropionic Acid-degrading Bacterium *Variovorax paradoxus*. *J. Biol. Chem. 284*, 660−672.
(61) Stipanuk, M., Simmons, C., Andrew Karplus, P., and Dominy, J. (2011) Thiol dioxygenases: Unique families of cupin proteins. *Amino Acids 41*, 91−102.
(62) Kabil, O., and Banerjee, R. (2012) Characterization of Patient Mutations in Human Persulfide Dioxygenase (ETHE1) Involved in H_2S Catabolism. *J. Biol. Chem. 287*, 44561−44567.
(63) Li, L., Rose, P., and Moore, P. K. (2011) Hydrogen Sulfide and Cell Signaling. *Annu. Rev. Pharmacol. Toxicol. 51*, 169−187.
(64) Gadalla, M. M., and Snyder, S. H. (2010) Hydrogen sulfide as a gasotransmitter. *J. Neurochem. 113*, 14−26.
(65) McCoy, J. G., Bingman, C. A., Bitto, E., Holdorf, M. M., Makaroff, C. A., and Phillips, G. N., Jr. (2006) Structure of an ETHE1-like protein from *Arabidopsis thaliana*. *Acta Crystallogr. D62*, 964−970.